

Cell-Type- and Endocannabinoid-Specific Synapse Connectivity in the Adult Nucleus Accumbens Core

Marion A. Deroche,^{1,2,3} Olivier Lassalle,^{1,2,3} Laia Castell,⁴ Emmanuel Valjent,⁴ and  Olivier J. Manzoni^{1,2,3}

¹Institut de Neurobiologie de la Méditerranée INMED, Institut National de la Santé et de la Recherche Médicale INSERM U1249, 13273 Marseille, France, ²Aix-Marseille University, 13273 Marseille, France, ³Cannalab, Cannabinoids Neuroscience Research International Associated Laboratory INSERM-Indiana University, Bloomington Indiana, and ⁴Institut de Génomique Fonctionnelle, Centre National de la Recherche Scientifique CNRS, INSERM, University of Montpellier, 34090 Montpellier, France

The nucleus accumbens (NAc) is a mesocorticolimbic structure that integrates cognitive, emotional and motor functions. Although its role in psychiatric disorders is widely acknowledged, the understanding of its circuitry is not complete. Here, we combined optogenetic and whole-cell recordings to draw a functional portrait of excitatory disambiguated synapses onto D1 and D2 medium spiny neurons (MSNs) in the adult male mouse NAc core. Comparing synaptic properties of ventral hippocampus (vHipp), basolateral amygdala (BLA) and prefrontal cortex (PFC) inputs revealed a hierarchy of synaptic inputs that depends on the identity of the postsynaptic target MSN. Thus, the BLA is the dominant excitatory pathway onto D1 MSNs (BLA > PFC = vHipp) while PFC inputs dominate D2 MSNs (PFC > vHipp > BLA). We also tested the hypothesis that endocannabinoids endow excitatory circuits with pathway- and cell-specific plasticity. Thus, whereas CB1 receptors (CB1R) uniformly depress excitatory pathways regardless of MSNs identity, TRPV1 receptors (TRPV1R) bidirectionally control inputs onto the NAc core in a pathway-specific manner. Finally, we show that the interplay of TRPV1R/CB1R shapes plasticity at BLA-NAc synapses. Together these data shed new light on synapse and circuit specificity in the adult NAc core and illustrate how endocannabinoids contribute to pathway-specific synaptic plasticity.

Key words: endogenous cannabinoids; accumbens; TRPV1R; CB1R

Significance Statement

We examined the impact of connections from the ventral hippocampus (vHipp), basolateral amygdala (BLA) and prefrontal cortex (PFC) onto identified medium spiny neurons (MSNs) in the adult accumbens core. We found BLA inputs were strongest at D1 MSNs while PFC inputs dominate D2 MSNs. Pathway- and cell-specific circuit control was also facilitated by endocannabinoids that endow bidirectional synaptic plasticity at identified BLA-NAc synapses. These data provide mechanistic insights on synapse and circuit specificity in the adult NAc core.

Introduction

The nucleus accumbens (NAc) is a mesocorticolimbic structure (Humphries and Prescott, 2010) that integrates cognitive, emotional and motor functions (Floresco, 2015). Although the NAc's role in neurological and psychiatric disorders including anxiety, depression, addiction and intellectual disability (Goto and Grace,

2008; Kasanetz et al., 2010; Sesack and Grace, 2010; Lafourcade et al., 2011; Jung et al., 2012; Neuhofner et al., 2015, 2018; Bosch-Bouju et al., 2016; Manduca et al., 2017) is widely acknowledged (Salgado and Kaplitt, 2015), a detailed understanding of its physiological mechanisms is lacking.

The NAc consists of at least two subregions, a medial “shell” region and a more lateral “core” component associated with the extended amygdala and the basal ganglia, respectively (Zahm and Brog, 1992). The core and shell have different morphology and serve different cognitive functions (Floresco, 2015; Salgado and Kaplitt, 2015; reward- and motivation-related learning, respectively). The principal cell type is GABAergic projection medium-spiny neurons (MSNs) which express either D1 or D2 receptors and play specific roles in NAc-mediated behaviors and disorders (Lobo and Nestler, 2011; Francis et al., 2015).

In young mice, MSNs' intrinsic and synaptic properties diverge: D2 MSNs are more excitable than D1. Whether these specific differences in MSNs persist in adulthood remains unknown.

Received May 14, 2019; revised Dec. 4, 2019; accepted Dec. 5, 2019.

Author contributions: M.A.D., O.L., E.V., and O.J.M. designed research; M.A.D., O.L., and L.C. performed research; M.A.D., O.L., L.C., and E.V. analyzed data; M.A.D. and O.J.M. wrote the first draft of the paper; M.A.D. and O.J.M. edited the paper; M.A.D., E.V., and O.J.M. wrote the paper.

This work was supported by the Institut National de la Santé et de la Recherche Médicale (INSERM); Fondation pour la Recherche Médicale (Equipe FRM 2015 to O.J.M.) and the National Institutes of Health (Grant R01DA043982). We thank Pascale Chavis and members of the Chavis-Manzoni laboratory for helpful discussions, Andrew Scheyer for correcting the manuscript, Steeve Maldera for experimental help, Daniela Neuhofner for initiating the project, and the National Institute of Mental Health's Chemical Synthesis and Drug Supply Program (Rockville, MD, USA).

The authors declare no competing financial interests.

Correspondence should be addressed to Olivier J. Manzoni at olivier.manzoni@inserm.fr.

<https://doi.org/10.1523/JNEUROSCI.1100-19.2019>

Copyright © 2020 the authors

NAc MSNs receive and integrate glutamatergic inputs, most notably from the prelimbic region of the prefrontal cortex (PFC), the ventral hippocampus (vHipp) and basolateral amygdala (BLA) (Groenewegen et al., 1999; Britt et al., 2012) but also from the thalamus, dorsal hippocampus, VTA and insular cortex (Stratford and Wirtshafter, 2013; Qi et al., 2016; Zhu et al., 2016; Rogers-Carter et al., 2019; Trouche et al., 2019). These regions process dissociable types of information and the specific activation of these pathways can elicit distinct behavioral functions via interactions with the NAc (Goto and Grace, 2008; Sesack and Grace, 2010). The PFC and the NAc interact in behaviors that require executive attention or working memory (Christakou et al., 2001, 2004; Cools et al., 2007), that place high demands on attention (Christakou et al., 2004), or necessitate the linking of behaviors across contexts (Floresco et al., 1999). The vHipp-NAc pathway is essential for spatial navigation in relation to goal direct behavior (Floresco et al., 1997; Ito et al., 2008; Mannella et al., 2013) and in encoding the temporal dynamics of decision making (Cardinal and Howes, 2005; Eichenbaum, 2014; Abela et al., 2015). By contrast, the BLA-NAc pathway plays a large role in conditioned emotional responses (Everitt et al., 2003; LeDoux, 2003; Tye et al., 2011; Beyeler et al., 2016, 2018) and in forming associations between stimuli that predict appetitive or aversive consequences (Everitt et al., 1991; McLaughlin and Floresco, 2007; Shiflett and Balleine, 2010; Fernando et al., 2013).

The mesocorticolimbic endocannabinoid (eCB) system modulates a vast array of synaptic functions (Robbe et al., 2002; Lafourcade et al., 2007; Araque et al., 2017). eCB-mediated long-term depression was originally discovered in the NAc/ventral striatum (Robbe et al., 2002) and dorsal striatum (Gerdeman et al., 2002). eCB dysfunction is implicated as a major causal factor in a plethora of synaptopathies linked to the NAc (Kasanez et al., 2010; Lafourcade et al., 2011; Jung et al., 2012; Neuhofer et al., 2015, 2018; Bosch-Bouju et al., 2016; Araque et al., 2017; Manduca et al., 2017). In the dorsal striatum, chemically induced eCB-synaptic plasticity shows pathway but not MSN subtype specificity (Wu et al., 2015). Whether eCBs contribute to pathway-specificity in the NAc and its mechanistic underpinnings is unknown. Here, we explored the innervation and synaptic properties of PFC, BLA and vHipp to the NAc core. In addition, we assayed each pathway for eCB receptors and dissected eCB-plasticity at BLA inputs. We report that adult D1- are inherently more excitable than D2 MSNs and that the hierarchy of excitatory inputs depends on the identity of the postsynaptic target MSN and on circuit specific properties. Finally, we provide evidence that the eCB system endows excitatory circuits of the NAc with pathway- and cell-specific plasticity. Together these data reveal a high degree of synapse and circuit specificity in the adult NAc core.

Materials and Methods

Animals. Animals were treated in compliance with the European Communities Council Directive (86/609/EEC) and the U.S. National Institutes of Health's *Guide for the Care and Use of Laboratory Animals*. The French Ethical committee authorized this project (APAFIS#3279-2015121715284829 v5). Male *Drd1a*-tdTomato mice were from The Jackson Laboratory and female C57BL/6J background mice were purchased from the Janvier Laboratory. Mice were acclimated to the animal facility for 1 week and then housed in male and female pairs to enable breeding of hemizygous offspring. Mice were ear punched for identification and genotyping. Mice were housed at constant room temperature ($20 \pm 1^\circ\text{C}$) and humidity (60%) and exposed to a light cycle of 12 h light/dark (08:00 A.M. to 08:00 P.M.), with *ad libitum* access to food and water. All experiments were performed on male offspring C57BL/6J mice between P100 and P130.

Injection of the virus. Microinjection needles (32 Ga) were connected to a 10 μl Hamilton syringe and filled with purified, concentrated adeno-associated virus (1.98×10^{13} infectious units per milliliter) encoding hChR2-EYFP under control of the CaMKII α promoter (University of Pennsylvania, Philadelphia). Mice were anesthetized with 150 mg/kg ketamine and 50 mg/kg xylazine and placed in a stereotaxic frame. Microinjection needles were bilaterally placed into the vHipp (coordinates: AP = -3.2 mm; ML = 2.85 mm; DV = 3.84 mm), basolateral amygdala (coordinates: AP = -1 mm; ML = 3.1 mm; DV = 3.9 mm) or prefrontal cortex (coordinates: AP = 2 mm; ML = 0.3 mm; DV = 2 mm) and 250 nL of virus was injected with a speed of 100 nL/min. The needles were left in place for an additional 5 min to allow for diffusion of virus particles away from injection site.

Slice preparation. Five to 6 weeks after surgery, adult male mice (P100–P130) were deeply anesthetized with isoflurane and killed as previously described (Robbe et al., 2002; Lafourcade et al., 2011; Jung et al., 2012; Neuhofer et al., 2018). The brain was sliced (300 μm) on the coronal plane with a vibratome (Integralslice, Campden Instruments) in a sucrose-based solution at 4°C containing the following (in mM): 87 NaCl, 75 sucrose, 25 glucose, 2.5 KCl, 4 MgCl_2 , 0.5 CaCl_2 , 23 NaHCO_3 and 1.25 NaH_2PO_4 . Immediately after cutting, slices containing the NAc were stored for 1 h at 32°C in a low-calcium ACSF containing the following (in mM): 130 NaCl, 11 glucose, 2.5 KCl, 2.4 MgCl_2 , 1.2 CaCl_2 , 23 NaHCO_3 , and 1.2 NaH_2PO_4 , equilibrated with 95% O_2 /5% CO_2 and then at room temperature until the time of recording. EYFP expression was examined in slices containing the virus injection sites to assess placement accuracy.

Electrophysiology. Whole-cell patch-clamp recordings of visualized NAc medium spiny neurons (MSNs) were made in coronal slices containing the NAc as previously described (Robbe et al., 2002; Lafourcade et al., 2011; Jung et al., 2012; Neuhofer et al., 2018). During the recording, slices were placed in the recording chamber and superfused at 2 ml/min with normal ACSF. All experiments were done at 25°C . The superfusion medium contained picrotoxin (100 μM) to block GABA type A (GABA-A) receptors, unless specified otherwise. All drugs were added at the final concentration to the superfusion medium.

For whole-cell patch-clamp experiments, neurons were visualized using an upright microscope with infrared illumination. The intracellular solution was based on K^+ gluconate containing the following (in mM): 145 K^+ gluconate, 3 NaCl, 1 MgCl_2 , 1 EGTA, 0.3 CaCl_2 , 2 Na^+ ATP, and 0.3 Na^+ GTP, 0.2 cAMP, buffered with 10 HEPES. The pH was adjusted to 7.2 and osmolarity to 290–300 mOsm. Electrode resistance was 4–6 $\text{M}\Omega$.

A -2 mV hyperpolarizing pulse was applied before each evoked EPSC to evaluate the access resistance, and those experiments in which this parameter changed $>25\%$ were rejected. Access resistance compensation was not used, and acceptable access resistance was <30 $\text{M}\Omega$. The potential reference of the amplifier was adjusted to zero before breaking into the cell. Cells were held at -70 mV.

Current–voltage (I – V) curves were made by a series of hyperpolarizing to depolarizing current steps immediately after breaking into the cell. Membrane resistance was estimated from the I – V curve around resting membrane potential (Kasanez et al., 2010; Thomazeau et al., 2014; Martin et al., 2017).

The paired-pulse ratio (PPR) was calculated from the peak current of two closely spaced EPSCs (50 ms), such that the $\text{PPR} = \text{Peak } 2/\text{Peak } 1$. Quoted PPR values are the average of 30 trials. For the measurements of quantal EPSCs (qEPSCs), transmitter release was desynchronized by substituting calcium with strontium (4 mM) in the superfused ACSF. Asynchronous EPSCs were examined during a 200 ms window beginning 5 ms after optical stimulation. Recordings were analyzed if the frequency of events in this 200 ms window were significantly greater than during the 200 ms window preceding the stimulation as previously described (Britt et al., 2012).

Optogenetics. A 473 nm laser (Dragon Laser) coupled to a 50 μm core glass silica optical fiber (ThorLabs) was positioned directly above the slice orientated at $30^\circ \sim 350$ μm from the recording electrode. At the site of recording discounting scattering a region of ~ 0.05 mm^2 was illuminated that after power attenuation due to adsorption and scattering in the tissue was calculated as ~ 100 mW/mm^2 (Yizhar et al., 2011). Optically evoked EPSCs were obtained every 10 s with pulses of 473 nm wavelength light (0–10 mW, 2 ms).

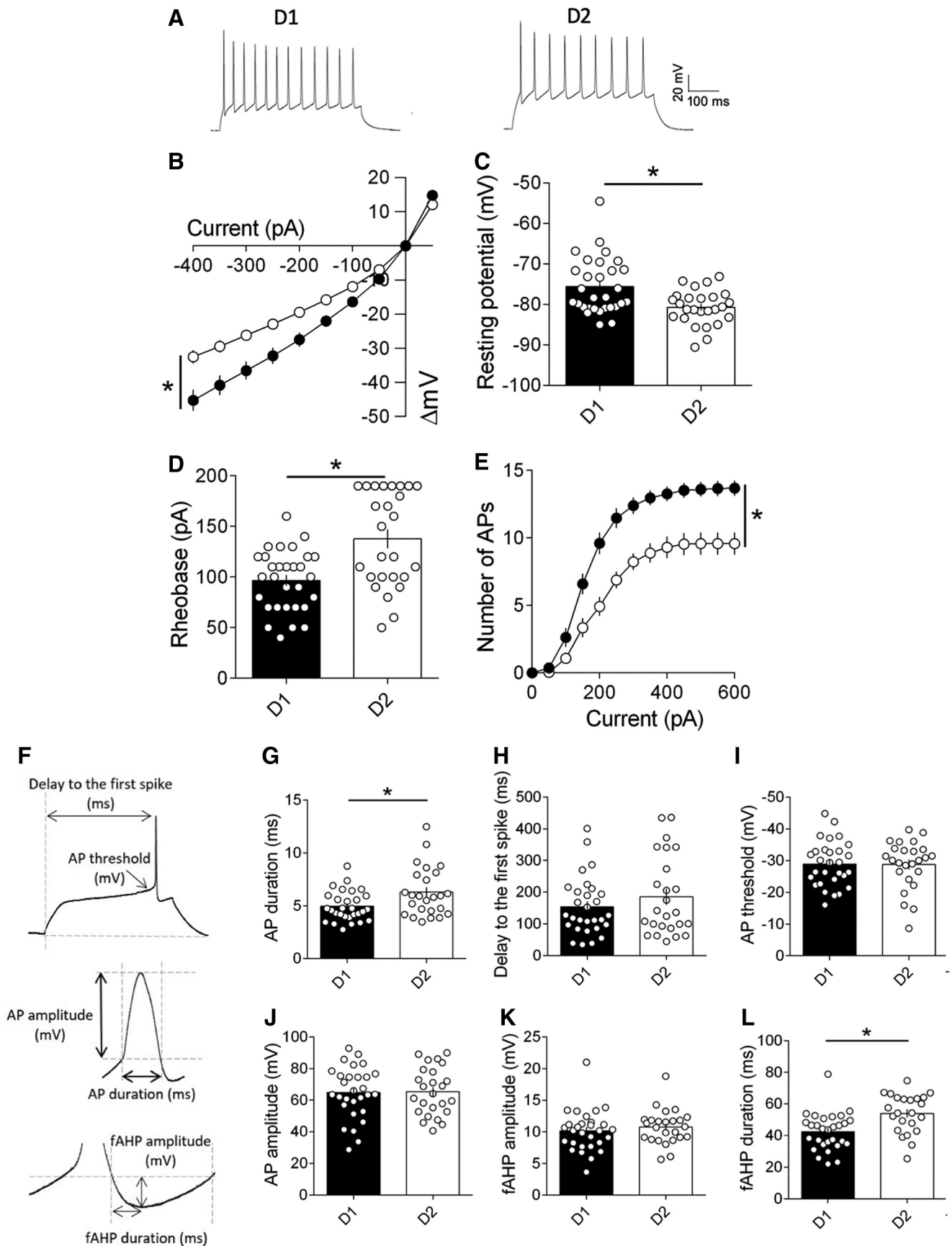


Figure 1. Adult NAc core D1 MSNs are more excitable than D2 MSNs. **A**, Typical membrane responses from NAc core D1 or D2 MSNs in reaction to a series of increasing somatic current injections. Sample spike trains in response to depolarizing current from D1 or D2 MSN. **B**, Summary of all the I - V curves recorded in D1 (black, $n = 30$) and D2 (white, $n = 26$) MSNs ($F_{(interaction\ 26,1404)} = 8.03$, $p < 0.0001$, $F_{(cell\ type\ 1,54)} = 2.893$, $p < 0.0001$, two-way repeated-measures ANOVA). **C**, The resting membrane potential of D2 MSNs was significantly (Figure legend continues.)

RNAscope ISH assay. Staining for *Drd1*, *Drd2* and *Trpv1* mRNAs was performed using single-molecule fluorescent *in situ* hybridization (smFISH). Brains from 2 C57BL/6J 8-week-old male mice were rapidly extracted and snap-frozen on dry ice and stored at -80°C until use. Ventral striatum coronal sections ($14\ \mu\text{m}$) were collected directly onto Superfrost Plus slides (Fisher Scientific). RNAscope Fluorescent Multiplex labeling kit (ACDBio catalog #320850) was used to perform the smFISH assay according to manufacturer's recommendations. Probes used for staining are mm-Trpv1-C1 (ACDBio catalog #313331), mm-Drd1-C2 (ACDBio catalog #461901-C2) and mm-Drd2-C3 (ACDBio catalog #406501-C3). After incubation with fluorescent-labeled probes, slides were counterstained with DAPI and mounted with ProLong Diamond Antifade mounting medium (Thermo Fisher Scientific catalog #P36961). Fluorescent images of labeled cells in the NAc Core (bregma 1.54 mm to 1.42 mm) were captured using sequential laser scanning confocal microscopy (Leica SP8).

Drugs. Drugs were added at the final concentration to the recording ACSF media. Picrotoxin, strontium, capsaicin, and tetrodotoxin were from Sigma-Aldrich; capsazepine and CP55,940 from Tocris Bioscience; CNQX and SR 141716 were from the National Institute of Mental Health's Chemical Synthesis and Drug Supply Program.

Data acquisition and analysis. Whole-cell patch-clamp recordings were performed with an Axopatch-200B amplifier as previously described (Robbe et al., 2002; Kasanetz and Manzoni, 2009; Lafourcade et al., 2011; Jung et al., 2012; Thomazeau et al., 2014, 2017; Martin et al., 2017). Data were low pass filtered at 2 kHz, digitized (10 kHz, DigiData 1440A, Molecular Devices), collected using Clampex 10.2 and analyzed using Clampfit 10.2 (all from Molecular Devices). The magnitude of plasticity was calculated and compared 25–30 min after induction.

Spontaneous and quantal AMPAR-mediated EPSCs (sEPSCs/qEPSCs) were recorded using Axoscope 10 (Molecular Devices). sEPSCs/qEPSCs were filtered at 2 kHz and digitized at 20 kHz. sEPSCs/qEPSCs amplitude and frequency were analyzed with Axograph X using a double exponential template: $f(t) = \exp(-t/\text{rise}) + \exp(-t/\text{decay})$, rise = 0.5 ms. The threshold of amplitude detection was set at 5 pA.

Statistics. Statistical analysis of data was performed with Prism (GraphPad Software 6.0) using tests indicated in the main text after outlier subtraction (ROUT test). *N* values represent cells or individual animals. All values are given as mean \pm SEM, and statistical significance was set at $*p < 0.05$.

Results

We recorded a total of 412 MSNs from the NAc core of 291 Tg (*Drd1a*-tdTomato) Calak hemizygous adult male mice (P100–P130). MSNs were either tdTomato-labeled “D1-positive” MSNs or tdTomato-unlabeled/presumably D1-negative MSNs. Because previous studies have consistently shown that unlabeled D1-negative MSNs are all D2-positive MSNs, in the remainder of the study, we refer to tdTomato-unlabeled MSNs as D2 MSNs (Bertran-Gonzalez et al., 2008; Ade et al., 2011; Enoksson et al., 2012; Thibault et al., 2013; Cao et al., 2018).

←

(Figure legend continued.) hyperpolarized compared with that of D1 MSNs ($p = 0.0051$, Mann–Whitney *U* test). **D**, The rheobase, the minimal current required to trigger an action potential, was much lower in D1 MSNs ($p = 0.0025$, Mann–Whitney *U* test). **E**, The number of evoked action potentials in response to increasing depolarizing current steps was larger in D1 MSNs compared with D2 MSNs ($F_{(\text{interaction } 12,648)} = 5.927, p < 0.0001, F_{(\text{cell type } 1,54)} = 27.38, p < 0.0001$, two-way repeated measure ANOVA). **F**, Example of individual AP evoked by depolarizing current injection, indicating delay to the first spike, AP threshold, AP amplitude, AP duration, fAHP amplitude and fAHP duration metrics. **G**, AP duration is shorter in D1 MSNs compared with D2 MSNs (D1 MSNs $n = 30$; D2 MSNs $n = 26, p = 0.0354$, Mann–Whitney *U* test). The following action potential properties did not vary between the MSN subtype: **H**) delay to the first spike, **I**) AP threshold, **J**) AP amplitude and **K**) fAHP amplitude. **L**, fAHP duration is increased in D2 MSNs compared with D1 MSNs ($p = 0.0009$ Mann–Whitney *U* test). Individual point in scatter dot plots represents one individual neuron. All data are shown as mean \pm SEM. $*p < 0.05$.

Intrinsic properties of D1 and D2 MSNs in adult *Drd1a*-tdTomato mice

In juvenile and adolescent mice, D2 MSNs are more excitable than D1 MSNs in the NAc (Grueter et al., 2010; Ma et al., 2014; Cao et al., 2018). To our knowledge, the intrinsic properties of D1 and D2 MSNs in adult NAc core have not been described previously.

The intrinsic properties of current-clamped and visually identified neighboring D1 and D2 MSNs were compared in NAc core slices from adult *Drd1a*-tdTomato mice (Fig. 1). The membrane reaction profiles of D1 and D2 MSNs in response to a series of somatic current steps differ greatly (Fig. 1B). Differences between MSN subtypes extended to their resting membrane potential, which was significantly more depolarized in D1 than D2 MSNs (Fig. 1C) and the rheobase was significantly lower in D1 than D2 MSNs (Fig. 1D). The hyperexcitability of D1 MSNs was accompanied by an increased number of action potentials in response to somatic currents steps in D1 compared with D2 MSNs (Fig. 1E). Action potential duration was also shorter in D1 MSNs and action potential afterhyperpolarization (fAHP) was larger in D2 MSNs (Fig. 1F–L). Thus, in the NAc core of adult mice, D1 MSNs are more excitable than D2 MSNs.

Cell-type-specific hierarchy of excitatory inputs in the adult NAc core

In postsynaptic NAc shell MSNs, optogenetic methods and targeted channelrhodopsin-2 (ChR2) expression to projection neurons from the ventral hippocampus (vHipp), basolateral amygdala (BLA) and prefrontal cortex (PFC) revealed that vHipp inputs elicit the largest excitatory currents (vHipp > BLA > PFC; Britt et al., 2012). At the strict anatomical level, the PFC preferentially projects to the NAc core, in contrast with the vHipp which preferentially projects to the shell. The BLA projects equally to both NAc core and shell (Li et al., 2018).

However, the functional hierarchy of specific excitatory synaptic inputs to identified MSN subtypes in the NAc core is largely unknown. Akin to Britt and collaborators (Britt et al., 2012), we targeted ChR2 expression to projection neurons in the vHipp, BLA and PFC to compare the functional strength and synaptic properties of these inputs onto identified D1 and D2 MSNs in the NAc core of adult mice.

Five to 6 weeks after viral infection with pAAV9-CaMKIIa-hChR2(H134R)-EYFP in the vHipp, BLA or PFC, strong expression of ChR2-EYFP was observed in the NAc core (Fig. 2A). To best mimic “real life” action potentials and avoid direct illumination of axon terminals, light pulses (473 nm) were delivered with a custom-made optical fiber placed $\sim 350\ \mu\text{m}$ from the recorded MSNs (Fig. 2B). Independently of input, light-evoked EPSCs (optical EPSCs, oEPSCs) were abolished in the presence of the ionotropic glutamate receptor antagonist CNQX ($20\ \mu\text{M}$) or the sodium channel blocker tetrodotoxin (TTX, $1\ \mu\text{M}$) (Fig. 2C). These control experiments show that oEPSCs are genuinely glutamate-mediated EPSCs induced after light-evoked activation of axonal Na^+ channels.

In the NAc shell, “regardless of which pathway was optically stimulated, oEPSCs were observed in >95% of recorded neurons” (quoted from Britt et al., 2012). In our experiments, the same held true (data not shown), regardless of MSN subtypes, suggesting that each MSN receives innervation from PFC, vHipp and BLA (Finch, 1996; Groenewegen et al., 1999; French and Totterdell, 2002, 2003; McGinty and Grace, 2009; Britt et al., 2012).

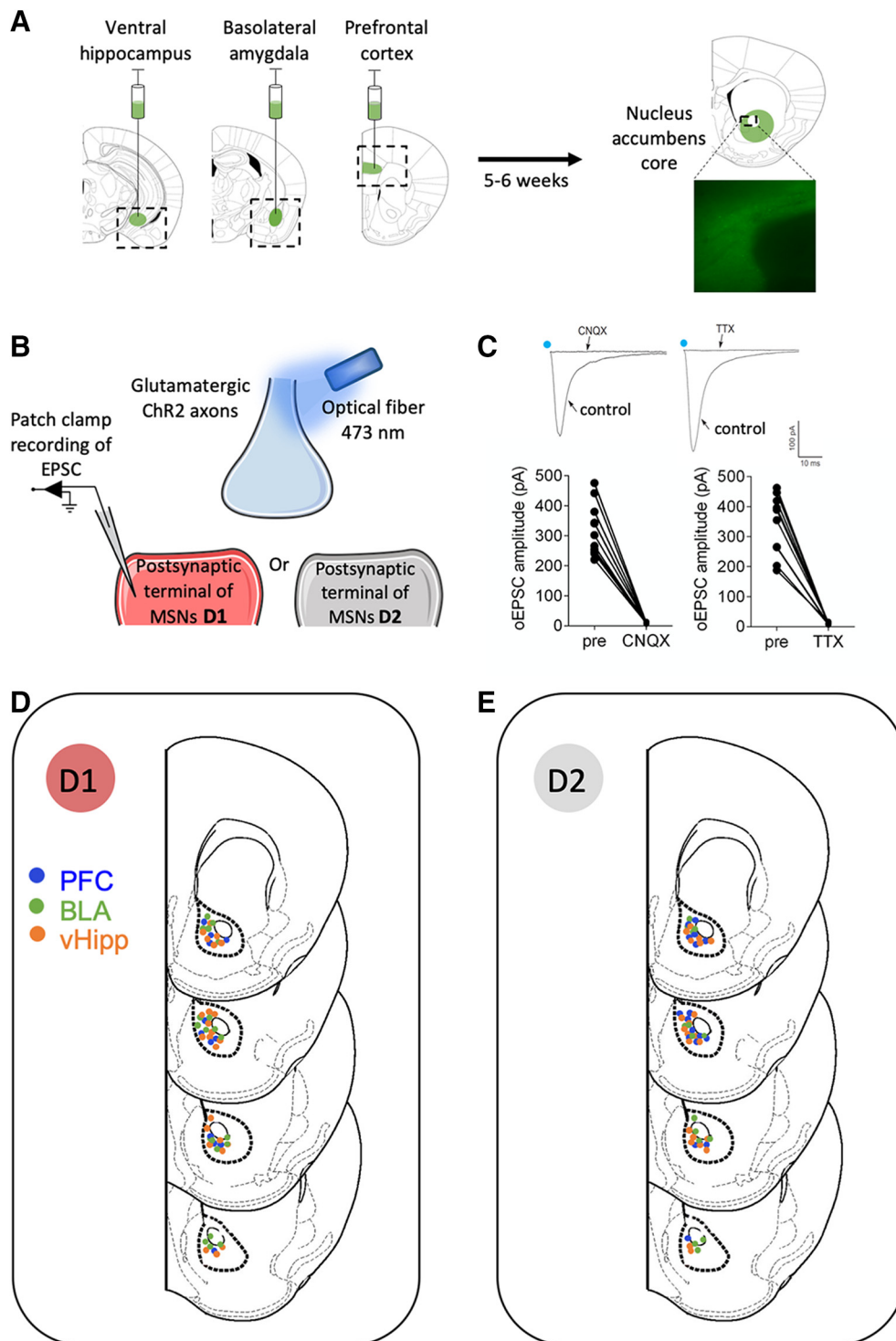


Figure 2. Pathway-specific evoked EPSCs in the Nac core after optical stimulation of ventral hippocampal, basal amygdala or prefrontal cortex inputs. **A**, Representative coronal brain slices showing expression of ChR2-eYFP (green) after injections of (0.25 μ l) AAV9.CaMKIIa.hChR2(H134R)-eYFP.WPRE.hGH (Addgene26969P; 1.98×10^6 GC/ml) in the vHipp, BLA, or PFC (left). Image of ChR2-EYFP expressing axons from principal (i.e., CaMKII expressing) cortical neurons (right). **B**, Illustration of the experimental setup. Synaptic terminals expressing ChR2-EYFP were stimulated with a 473 nm laser coupled to an optical fiber placed 350 μ m from the recording area. Recordings of optically evoked EPSCs were recorded in the whole-cell patch-clamp configuration in MSNs from the Nac core. **C**, Inward currents evoke by light stimulation in Nac core MSNs. CNQX (20 μ M) and TTX (1 μ M) completely prevented evoked currents recorded in the presence of PTX after optical stimulation of PFC inputs, showing that the oEPSCs depended on presynaptic and postsynaptic glutamate ionotropic AMPAR receptor-mediated currents. Individual oEPSCs amplitude experiments before (pre) and after CNQX ($n = 10$) or TTX ($n = 9$). Blue dots indicate optical stimulations. **D, E**, Location of whole-cell patch-clamped MSNs sorted by subtype in nucleus Nac core of Drd1-tdTomato transgenic mice. D1, Recordings from fluorescently labeled D1-positive MSNs (**D**); D2, recordings from nonfluorescently labeled MSNs (**E**).

Using increasing optical stimulations and whole-cell patch-clamp of visually identified MSNs, we built and compared input-output curves for PFC, BLA and vHipp inputs at both D1 and D2 MSNs (Fig. 3; see also Fig. 6). We compared evoked oEPSCs in

response to increasing stimulation intensity in different pathways across D1 and D2 MSNs (Fig. 3). We found that, when excitatory currents were elicited by optical stimulation of PFC fibers, the largest oEPSCs were observed at D2 MSNs (Fig. 3A–D). Similar

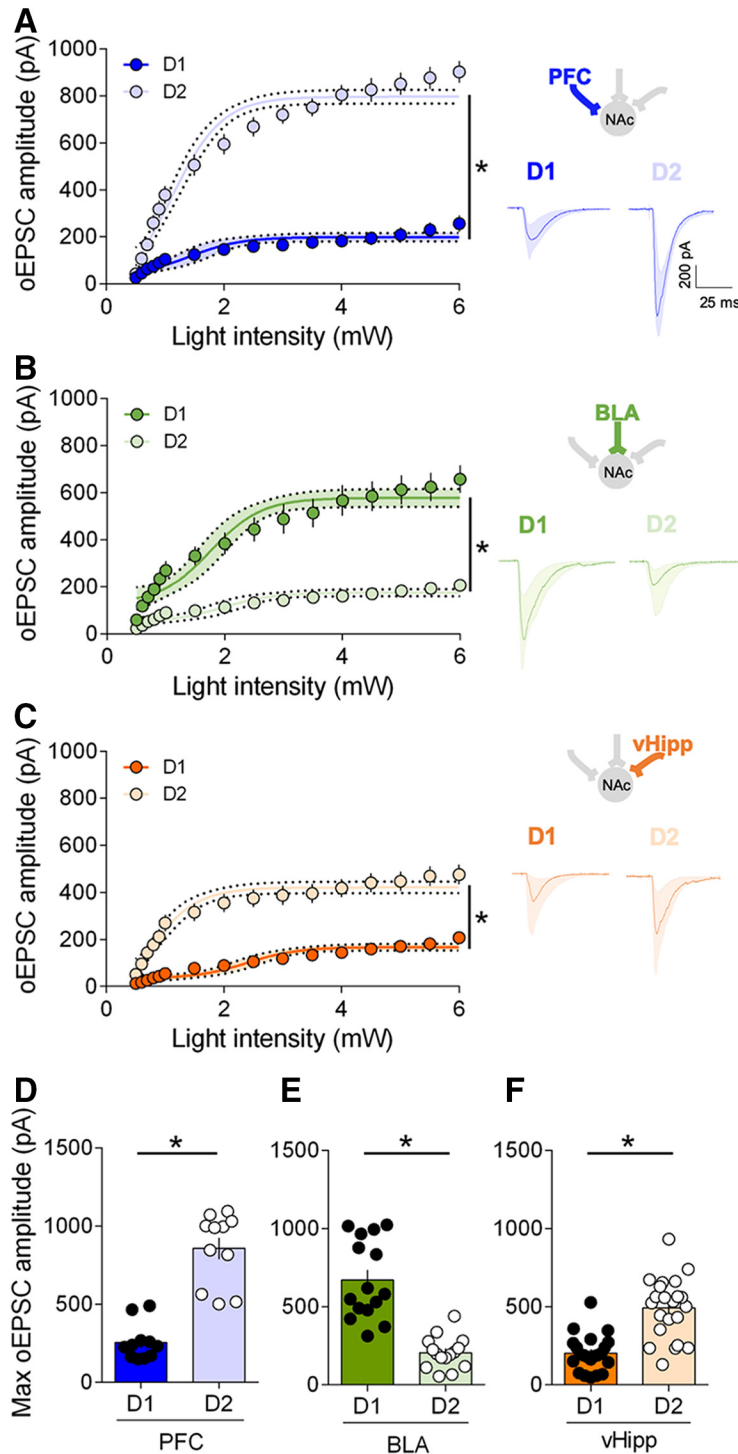


Figure 3. Hierarchy of optically driven synaptic inputs depends on the cellular identity of the target MSNs. **A**, Left, At PFC fibers, the largest excitatory oEPSCs in response to increasing light stimulations were recorded in D2 MSNs (light blue, $n = 17$) compared with D1 MSNs (dark blue, $n = 11$) ($F_{(interaction\ 15,416)} = 18.59, p < 0.0001, F_{(cell\ type\ 1,416)} = 934.4, p < 0.0001$, two-way repeated measure ANOVA). Right, Example oEPSC traces for PFC inputs onto D1 and D2 MSNs. **B**, Left, At BLA fibers, the largest excitatory oEPSCs in response to increasing light stimulations were recorded in D1 MSNs (dark green, $n = 20$) compared with D2 MSNs (light green, $n = 15$) ($F_{(interaction\ 15,528)} = 5.628, p < 0.0001, F_{(cell\ type\ 1,528)} = 331.5, p < 0.0001$, two-way repeated measure ANOVA). Right, Example oEPSC traces for BLA inputs onto D1 and D2 MSNs. **C**, Left, At vHipp fibers, the largest excitatory oEPSCs in response to increasing light stimulations were recorded in D2 MSNs (light orange, $n = 22$) compared with D1 MSNs (dark orange, $n = 24$) ($F_{(interaction\ 15,704)} = 4.310, p < 0.0001, F_{(cell\ type\ 1,704)} = 491.3, p < 0.0001$, two-way repeated measure ANOVA). Right, Example oEPSC traces for vHipp inputs onto D1 and D2 MSNs. **D**, Summary bar histogram showing maximum oEPSCs at PFC inputs onto D1 and D2 MSNs. (D1 MSNs $n = 11$, D2 MSNs $n = 11$, $p < 0.0001$, Mann–Whitney U test). **E**, Summary bar histogram of maximum oEPSCs at BLA inputs in neighboring D1 and D2 MSNs (D1 MSNs $n = 15$, D2 MSNs $n = 15$, $p < 0.0001$, Mann–Whitney U test). **F**, Summary bar histogram of maximum oEPSCs at vHipp inputs in neighboring D1 and D2 MSNs neighboring (D1 MSNs $n = 22$, D2 MSNs $n = 22$, $p < 0.0001$, Mann–Whitney U test). Individual point in scatter dot plots represents one individual neuron.

experiments performed at BLA and vHipp inputs showed that BLA-D1 > BLA-D2 (Fig. 3B–E) and vHipp-D2 > vHipp-D1 (Fig. 3C–F). These data show that in the adult NAc core, the hierarchy of synaptic inputs is specific to the cellular identity of the target MSNs.

Input- and cell-type-specific drive of action potential firing in the adult NAc core

What is the relationship between maximal excitatory synaptic strength and action potential firing of identified MSNs? We first sought to determine whether the pathway/cell specificity extended to the ability of different pathways to drive postsynaptic action potentials in identified MSNs. Current-clamp recordings revealed that optical recruitment of PFC inputs elicited postsynaptic action potentials with greater probability in D2 than D1 MSNs (Fig. 4A). In marked contrast, BLA inputs onto D1 MSNs were more likely to trigger action potentials than those onto D2 MSNs (Fig. 4B). Finally, there was no difference at vHipp inputs (Fig. 4C). Performed in the absence of inhibition, i.e., in the presence of picrotoxin, these results faithfully mirror the aforementioned cell-type-specificity of the hierarchy of synaptic strength.

Input- and cell-type-specific synaptic properties in the adult NAc core

To investigate cell-type-specific connectivity at glutamatergic inputs into the NAc, we compared postsynaptic and presynaptic parameters at disambiguated synapses in the NAc core. First, we measured the paired-pulse ratio (PPR), a classical index of neurotransmitter release probability (Silver et al., 1998) (Fig. 5A, B). In D1 MSNs, BLA inputs had a low PPR/high release probability and the highest PPR/lowest release probability was found at PFC inputs (D1: BLA > vHipp > PFC). In contrast, in D2 MSNs, PFC inputs exhibited the highest release probability, respectively, whereas the lowest probability of release was found at BLA inputs (D2: PFC = vHipp > BLA).

In immature mice, miniature EPSCs properties were similar in D1 and D2 MSNs in early life (P16–P24, Cao et al., 2018), whereas ~P42 sEPSCs are more

← The line between dots shows neighboring D1 and D2 neurons that were recorded in the same slice with the same optical fiber position. All data are shown as mean ± SEM or geometric mean ± CI. * $p < 0.05$.

frequent in D2 MSNs (Ma et al., 2012) in disagreement with an earlier report of higher miniature EPSCs in D1 MSNs (P28–P56, Grueter et al., 2010). We recorded sEPSCs in D1 and D2 NAc core MSNs of adult mice (Fig. 5C,D). The amplitude of the sEPSCs measured in D1 MSNs was slightly larger than that measured in D2 MSNs (in agreement with Grueter et al., 2010). Both MSN subtypes exhibited similar distribution and average interevent intervals.

Next, we measured light-evoked input-specific quantal EPSCs (qoEPSCs) by replacing our extracellular medium's calcium with strontium to desynchronize transmitter release (Britt et al., 2012; McGarry and Carter, 2017). qoEPSC amplitude provides a direct estimate of post-synaptic efficacy measure and qoEPSC frequency was taken as an indirect indication of the number of connections (Goda and Stevens, 1994).

At PFC and vHipp inputs, qoEPSC frequencies were similar across cell types (Fig. 5E,F). However, qoEPSC frequencies were larger at BLA-D2 than BLA-D1 synapses (Fig. 5G,H). In contrast, qoEPSC amplitude were larger at PFC-D1 and BLA-D2 synapses compared with the other afferents (Fig. 5G,H).

The large qoEPSC frequency and amplitude observed at BLA-D2 synapses may at first appear to be at odds with the high PPR/release probability at these synapses as estimated by our input/output experiments (Fig. 3). Although asynchronous events are considered “calcium-independent” (i.e., no calcium is present), strontium desynchronization is most likely the result of strontium's low-affinity binding to the calcium sensor underlying excitation/secretion coupling. Thus, differences in calcium-dependent processes in the terminals (e.g., posttranslational modification) may account for the difference between these two techniques. Another cautious interpretation of the results is that high quantal size and low Pr combine to yield a “weak” synapse.

Pathway-specific expression of CB1R and TRPV1R receptors

The eCB system modulates synaptic circuits in the CNS and notably the dorsal and ventral striatum (Araque et al., 2017). Inhibitory CB1 receptors (CB1Rs) have long been described at glutamatergic NAc core synapses using standard electrical stimulation (Robbe et al., 2001). Stimulation of CB1Rs with a submaximal dose of a synthetic cannabimimetic (CP55940 1 μ M, Fig. 6A,B) inhibited oEPSC in D1 and D2 MSNs regardless of the input pathway, in support of the idea that functional CB1R are present at all of these inputs. The degree of inhibition induced by the single dose used here, however, was pathway dependent. Thus, CP55940-induced inhibition was larger at BLA than PFC

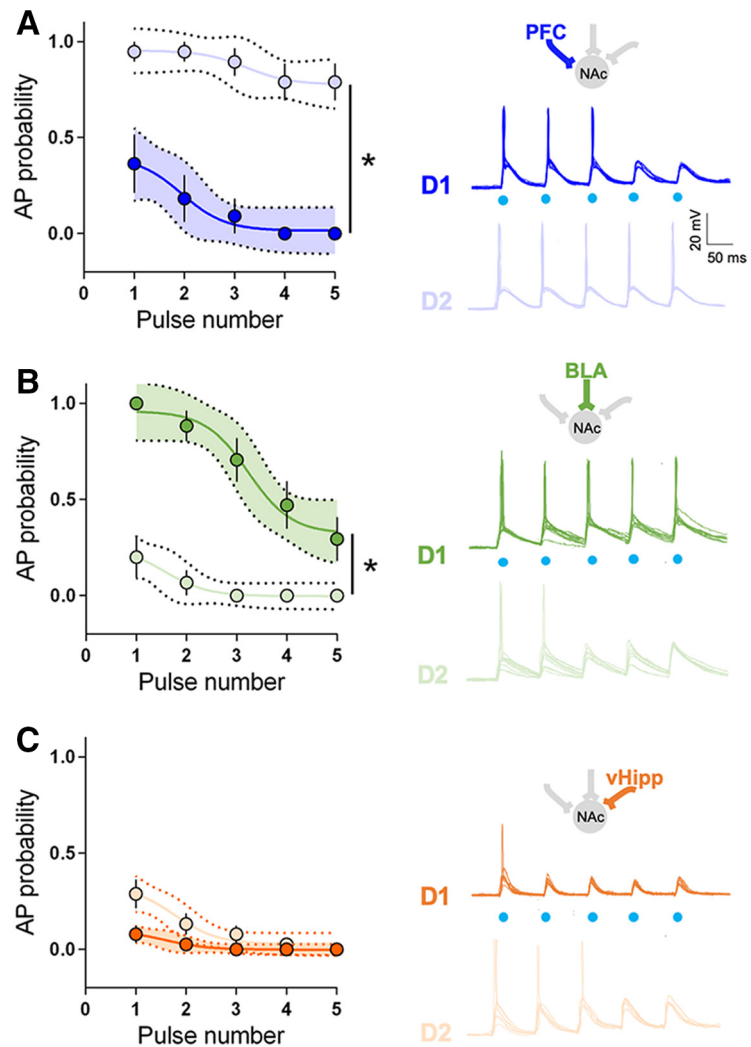


Figure 4. Pathway-specific drive of action potential in identified NAc core MSNs. **A**, Left, Comparison of the probability of AP firing versus pulse number shows that PFC inputs preferentially drive the firing of D2 MSNs compared with D1 MSNs (D1 MSNs $n = 6$, D2 MSNs $n = 6$, pulse 1: $p = 0.0005$, pulse 2–5: $p < 0.0001$, Fisher's exact test). Right, Example traces of APs evoked in D1 and D2 MSNs in response to trains of optical stimulation of PFC inputs (2 ms light pulses, 5 pulses at 10 Hz). **B**, Left, Comparison of the probability of AP firing versus pulse number shows that BLA inputs preferentially drive the firing of D1 MSNs compared with D2 MSNs (D1 MSNs $n = 7$, D2 MSNs $n = 6$, pulse 1–3: $p < 0.0001$, pulse 4: $p = 0.0027$, pulse 5: $p = 0.0445$, Fisher's exact test). Right, Example traces of APs evoked in D1 and D2 MSNs in response to trains of optical stimulation of BLA inputs. **C**, Left, Comparison of the probability of AP firing versus pulse number shows no difference at vHipp inputs of the firing of D1 MSNs and D2 MSNs (D1 MSNs $n = 6$, D2 MSNs $n = 6$, pulse 1: $p = 0.0357$, pulse 2: $p = 0.1997$, pulse 3–5: $p = 1.0000$, Fisher's exact test). Right, Example traces of APs evoked in D1 and D2 MSNs in response to trains of optical stimulation of vHipp inputs. Blue dots indicate time of stimulation. All experiments were performed in the presence of picrotoxin to prevent from feedforward inhibition. All data are shown as mean \pm SEM or geometric mean \pm CI. * $p < 0.05$.

or vHipp-D1 synapses (Fig. 6C) and smaller at vHipp-D2 synapses (compared with PFC and BLA, Fig. 6D).

The nonselective cation channel, transient receptor potential cation channel subfamily V member 1 (TRPV1R), is a multifaceted mediator of eCB signaling in the CNS (Gibson et al., 2008; Manduca et al., 2017; Bara et al., 2018), notably in the striatum: pharmacological activation of TRPV1R suppresses and facilitates transmitter release in the dorsal striatum (Musella et al., 2009) and inhibits excitatory inputs onto D2 NAc core MSNs (Grueter et al., 2010). Multiple inputs onto D1 and D2 MSNs differentially expressing various levels of TRPV1R could explain these apparently contradicting results. Thus, we compared the effects of the specific TRPV1R agonist capsaicin in the disambiguated NAc core synapse preparation (Fig. 7). Although capsaicin inhibited

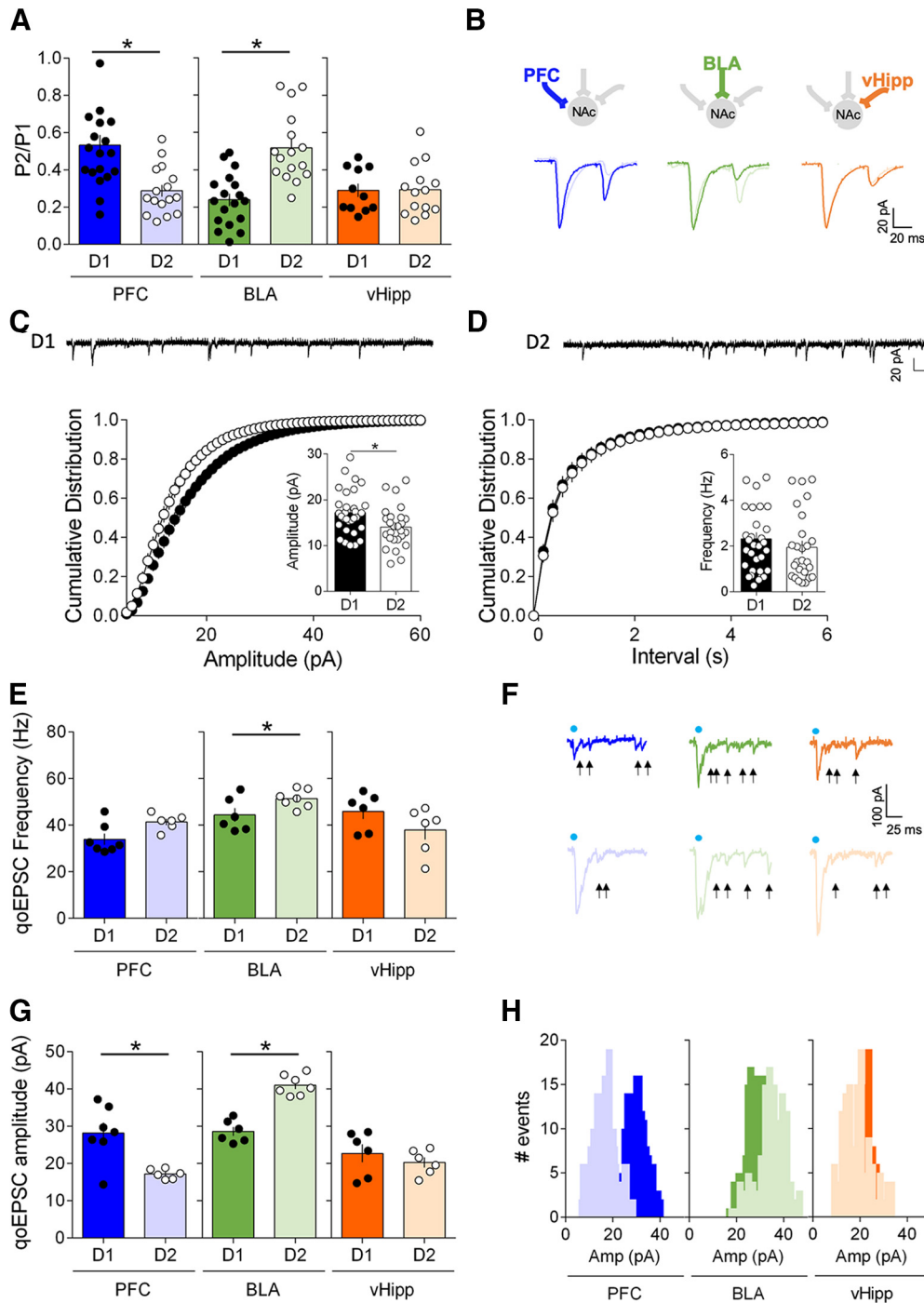


Figure 5. Input- and cell-type-specific postsynaptic and presynaptic properties in the NAc core. **A**, Average paired-pulse ratio (P2/P1) measured in D1 and D2 MSNs (voltage-clamp, -70 mV) in response to paired optical stimulations (50 ms interval) of PFC, BLA and vHipp inputs. PFC inputs had a lower PPR/high release probability in D2 MSNs (light blue) compared with D1 MSNs (dark blue) (D1 MSNs $n = 12$, D2 MSNs $n = 19$, $p = 0.0006$, Mann–Whitney U test). BLA inputs had a lower PPR/high release probability in D1 MSNs (dark green) compared with D2 MSNs (light green) (D1 MSNs $n = 16$, D2 MSNs $n = 18$, $p < 0.0001$, Mann–Whitney U test). vHipp inputs exhibited similar release probability in both D1 (dark orange) and D2 MSNs (light orange) (vHipp: D1 MSNs $n = 15$, D2 MSNs $n = 11$, $p > 0.9999$, Mann–Whitney U test). **B**, Example traces of evoked paired oEPSC responses to optical stimulations of PFC, BLA and vHipp inputs recorded in D1 MSNs and D2 MSNs. **C**, Left, Cumulative probability plot of measured sEPSC event amplitudes. Summary bar chart shows mean AMPAR event sEPSC amplitude (D1 MSNs: $n = 32$; D2 MSNs: $n = 26$, $p = 0.0146$, Mann–Whitney U test). Right, Cumulative probability plot of interval between measured sEPSC events. Scatter dot plots represents one cell. Summary bar chart shows mean AMPAR event sEPSC interval. **D**, Left, Light-evoked input-specific quantal EPSCs (qoEPSC) in the adult NAc. At BLA inputs, qoEPSCs frequencies were larger in D2 MSNs compared with D1 MSNs (D1 MSNs $n = 6$, D2 MSNs $n = 7$, $p = 0.0734$, Mann–Whitney U test). At PFC and vHipp inputs, qoEPSCs frequencies were similar in D1 MSNs and D2 MSNs (PFC: D1 MSNs $n = 7$, D2 MSNs $n = 6$, $p = 0.0361$; vHipp: D1 MSNs $n = 6$, D2 MSNs $n = 6$, $p = 0.1429$, Mann–Whitney U test). **E**, Representative qoEPSCs recorded in D1 MSNs and D2 MSNs in response to pathway specific opto-stimulation (arrows indicate detected qoEPSCs). **F**, At PFC inputs, qoEPSCs amplitudes were larger in D1 MSNs compared with D2 MSNs (D1 MSNs $n = 7$, D2 MSNs $n = 6$, $p = 0.0350$, Mann–Whitney U test). At BLA inputs, qoEPSCs amplitudes were larger in D2 MSNs compared with D1 MSNs (D1 MSNs $n = 6$, D2 MSNs $n = 7$, $p = 0.0012$, Mann–Whitney U test). At vHipp inputs, qoEPSC amplitudes were similar in D1 MSNs and D2 MSNs (D1 MSNs $n = 6$, D2 MSNs $n = 6$, $p = 0.1429$, Mann–Whitney U test). **G**, Histograms for representative D1 cells and D2 cells showing the distribution of qoEPSC amplitude across all trials. Blue dots indicate optical stimulations. Individual point in scatter dot plots represents one individual neuron. All data are shown as mean \pm SEM. * $p < 0.05$.

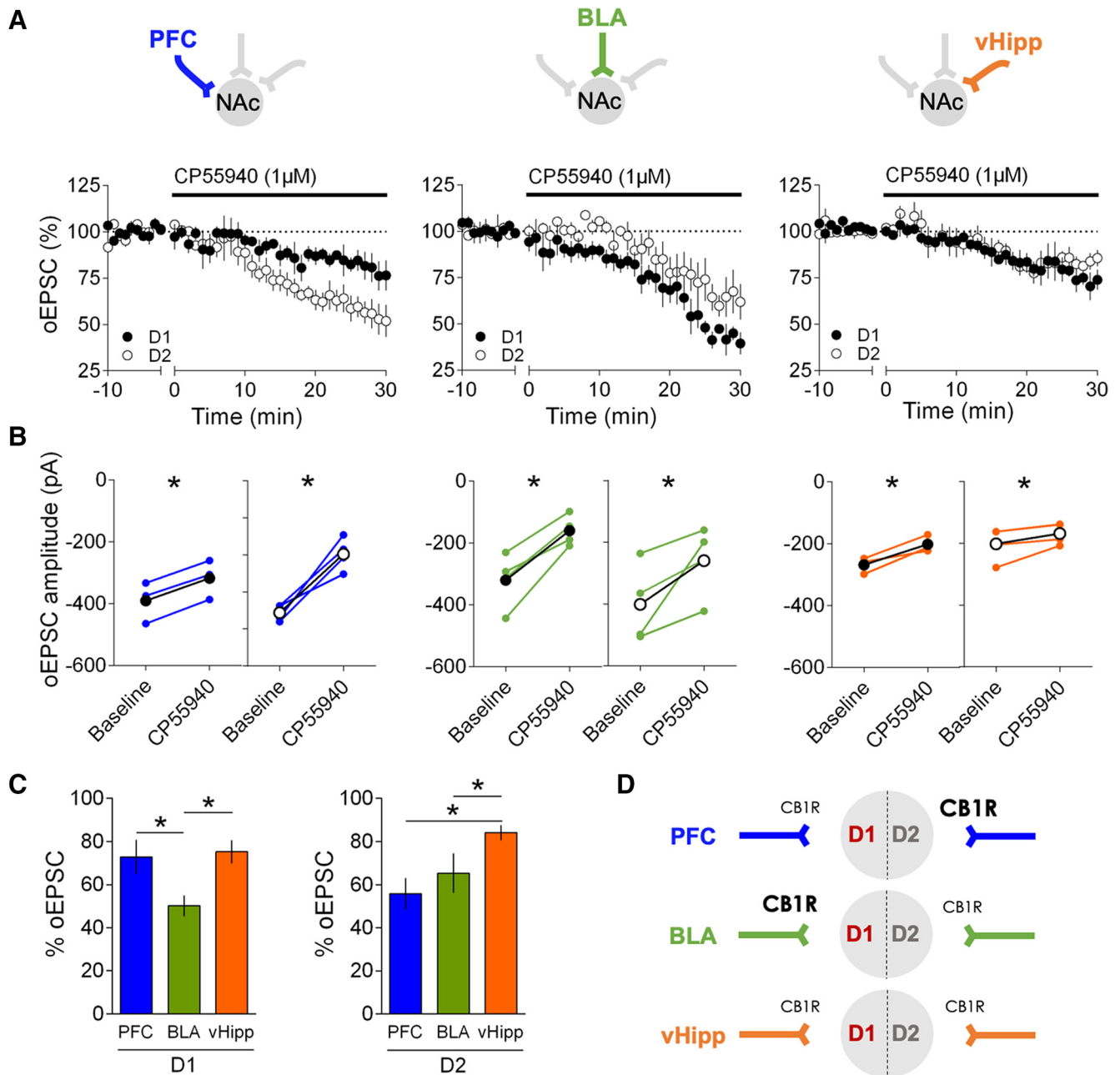


Figure 6. CB1R inhibition is common to all inputs onto D1 and D2 NAc core MSNs. **A**, Bath application of the synthetic CB1R agonist CP55940 (1 μ M), inhibited oEPSC in D1 (black) and D2 (white) MSNs. CP55940 was applied for 30 min (black bar) after at least 10 min of stable baseline recording. **B**, Individual and averaged oEPSCs amplitude experiments before (baseline) and 25–30 min after CP55940. (D1 MSNs, black circles: PFC $n = 3$, $p = 0.0014$, BLA $n = 4$, $p = 0.0110$, vHipp $n = 3$, $p = 0.0411$; D2 MSNs, white circles: PFC $n = 4$, $p = 0.0114$, BLA $n = 4$, $p = 0.0188$, vHipp $n = 4$, $p = 0.0496$ paired t test). **C**, Summary bar histogram comparing CP55940-induced inhibition of oEPSCs at identified PFC, BLA and vHipp inputs onto D1 (PFC $n = 3$, BLA $n = 4$, vHipp $n = 3$, $F_{(\text{input}, 2,7)} = 14.32$, $p = 0.0034$, one-way ANOVA) and D2 MSNs (PFC $n = 4$, BLA $n = 4$, vHipp $n = 4$, $F_{(\text{input}, 2,9)} = 4.207$, $p = 0.0513$, one-way ANOVA). **D**, Schematic view of the relative weight of CB1R-mediated inhibition at PFC, BLA and vHipp inputs onto D1 and D2 MSNs. n represents the number of mice. All data are shown as mean \pm SEM. * $p < 0.05$.

PFC-evoked oEPSCs in both D1 and D2 MSNs (Fig. 7*A, B*, left), the TRPV1R agonist had multifaceted effects on the other pathways. Capsaicin had opposite effects on BLA-evoked oEPSCs depending on the MSN subtype: the efficacy of BLA D1 MSN synapses was enhanced in the presence of the TRPV1 agonist but reduced at BLA-D2 MSNs synapses (Fig. 7*A, B*, middle). Finally, at vHipp inputs, TRPV1R activation specifically inhibited vHipp-D1 synapses and had no effect at vHipp synapses onto D2 MSNs (Fig. 7*A, B*, right). These results are summarized in Figure 7*D*.

At excitatory inputs in the NAc core, CB1R are expressed presynaptically (Robbe et al., 2001; Micale et al., 2009) and me-

diate presynaptic retrograde LTD (Robbe et al., 2002) while TRPV1R are localized postsynaptically (Micale et al., 2009) and trigger postsynaptic LTD specifically in D2 MSNs (Grueter et al., 2010; Neuhofer et al., 2018). We combined electrophysiological and RNAscope approaches to identify TRPV1R's loci of expression in our model. Capsaicin had opposite effects on spontaneous EPSCs recorded in D1 and D2 MSNs. In D1 MSNs the TRPV1R agonist reduced the frequency of spontaneous EPSCs (Fig. 8*A*), but not their amplitude, in support of a presynaptic localization (Fig. 8*B*). In D2 MSNs, however, capsaicin reduced the amplitude of spontaneous EPSCs (Fig. 8*B*), but not

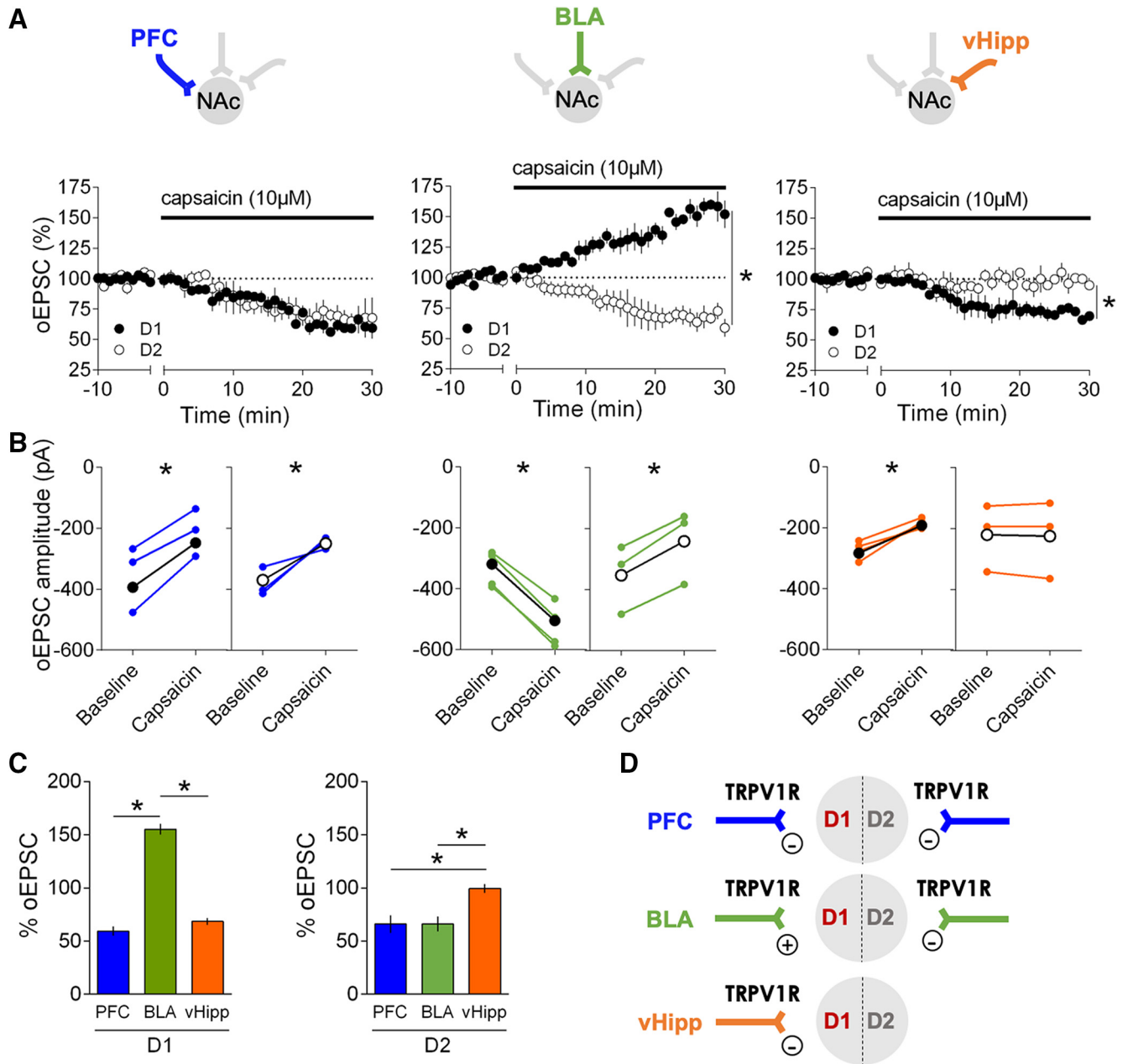


Figure 7. Divergent input- and cell-specific control of excitatory NAc synapses by TRPV1R. **A**, Effects of the TRPV1R agonist capsaicin (10 μ M) on oEPSCs at PFC, BLA, and vHipp synapses onto D1 (black circles) and D2 (white circles) MSNs. Capsaicin was applied for 30 min (black bar) after at least 10 min baseline recording. Capsaicin inhibited PFC-evoked oEPSCs similarly in both D1 (black) and D2 (white) MSNs. Capsaicin enhanced BLA-D1 MSN synapses but inhibited BLA-D2 MSN synapses. Finally, capsaicin inhibited vHipp-D1 MSN synapses and has no effect at vHipp-D2 MSN synapses. **B**, Individual and averaged oEPSCs amplitude experiments 10 min before (baseline) and 25–30 min after capsaicin; D1 MSNs, black circles: PFC $n = 3, p = 0.0308$, BLA $n = 4, p = 0.0188$, vHipp $n = 5, p = 0.0010$; D2 MSNs, white circles: PFC $n = 3, p = 0.0135$, BLA $n = 3, p = 0.0087$, vHipp $n = 3, p = 0.0109$ paired t test). **C**, Summary bar histogram of the maximal effects of capsaicin on oEPSCs at identified inputs onto D1 (PFC $n = 3$, BLA $n = 4$, vHipp $n = 5, F_{(input, 2, 9)} = 157.4, p < 0.0001$, one-way ANOVA) and D2 MSNs (PFC $n = 3$, BLA $n = 3$, vHipp $n = 3, F_{(input, 2, 6)} = 8.586, p = 0.0174$, one-way ANOVA). **D**, Schematic view of the relative weight and effects of TRPV1R on oEPSCs at PFC, BLA and vHipp inputs onto D1 and D2 MSNs. n represents the number of mice. All data are shown as mean \pm SEM. * $p < 0.05$.

their frequency (Fig. 8A), in support of a postsynaptic localization. These functional observations were corroborated by the distribution of *Trpv1*, *Drd1* and *Drd2* mRNAs. Triple staining indicated that in the NAc core, *Trpv1* mRNA was preferentially enriched in D2 MSNs compared with D1-expressing MSNs (Fig. 8C).

Together, these results reveal that whereas CB1R are uniformly expressed across input pathways onto D1/D2 MSNs, TRPV1R modulate excitatory inputs to the NAc core in a pathway- and cell-type-specific manner.

Cell-type-specific endocannabinoid-mediated LTD at amygdala synapses

In the last series of experiments, we focused on the BLA-NAc core synapses. These synapses are instrumental to reward-seeking behavior (Ambroggi et al., 2008) and have a role in positive emotional valence (Beyeler et al., 2018). Our present observation that both TRPV1R and CB1R modulate synaptic transmission in a cell-type-specific manner raised the possibility that the eCB interplay controls the polarity of activity-dependent plasticity at BLA-NAc synapses.

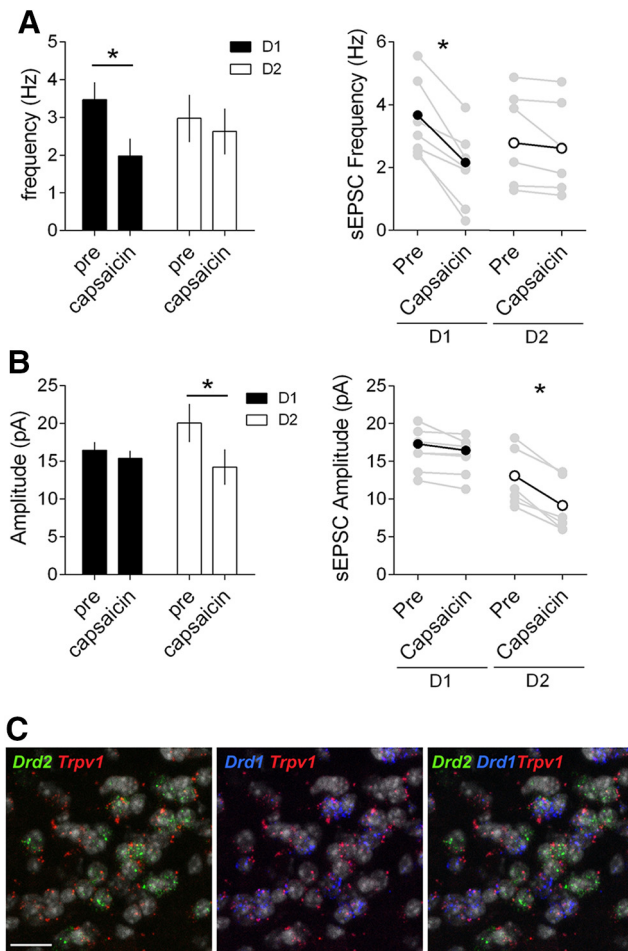


Figure 8. MSN-subtype-selective expression and function of TRPV1R in the NAc core. **A**, Left, Capsaicin reduces the frequency of sEPSC and in D1 but not D2 MSNs. Summary bar histogram comparing the mean sEPSC frequencies in D1 (black, $n = 7$) and D2 (white, $n = 6$) MSNs before and after capsaicin ($10 \mu\text{M}$). Right, Individual and averaged sEPSCs frequency experiments before (pre) and 25–30 min after capsaicin (D1 MSNs black circles, $p = 0.0013$ paired t test; D2 MSNs white circles $p = 0.1152$ paired t test). **B**, Left, Capsaicin reduces the amplitude of sEPSC in but not D1 MSNs. Summary bar histogram compares the mean sEPSC amplitudes in D1 (black, $n = 7$) and D2 (white, $n = 6$) MSNs before and after capsaicin. Right, individual and averaged sEPSCs amplitude (D) experiments before (pre) and 25–30 min after capsaicin (D1 MSNs black circles, $p = 0.0559$ paired t test; D2 MSNs white circles $p = 0.0008$ paired t test). All data are shown as mean \pm SEM. $*p < 0.05$ paired t test. **C**, Single-molecular fluorescent *in situ* hybridization for *Drd1* (blue), *Drd2* (green), and *Trpv1* (red) mRNAs in the NAc core. Slides were counterstained with DAPI (white). Scale bar, 12 μm . Note the segregation of cells expressing *Drd1* and *Drd2* mRNAs and the enrichment of *Trpv1* mRNA in D2 MSNs.

In the striatum, the principal form of eCB-mediated synaptic plasticity is LTD (Gerdeman et al., 2002; Robbe et al., 2002). We first compared the expression of eCB-LTD at BLA-D1 and -D2 synapses. Using the canonical protocol that elicits eCB-LTD in NAc MSNs (Robbe et al., 2002), we observed a robust LTD in D2 but not D1 MSNs after optical stimulation (Fig. 9). This is, to our knowledge, the first evidence that eCB-LTD can be optogenetically induced at a single set of identified synapses. Although this experiment can be interpreted as a lack of eCB-LTD at BLA inputs onto D1 MSNs, the current pharmacological characterization and previous work in the NAc core (Neuhofer et al., 2018) led us to test the possibility of another, more complex scenario. Based on the enhancing effects of the TRPV1R agonist at BLA-D1 synapses, we hypothesized that tetanus-induced eCB release (presumably anandamide) and the ensuing potentiation masked/

prevented the induction of LTD. In support of this idea we observed that in the presence of a TRPV1R antagonist (capsazepine, CPZ $10 \mu\text{M}$) the otherwise inefficacious protocol triggered a large LTD (Fig. 9C,D). Interestingly, bath application of the CB1R antagonist SR 141716 ($5 \mu\text{M}$) prevented the induction of LTD in the presence of CPZ (Fig. 9C,D).

The mirror situation was observed at BLA-D2 synapses. There, LTD was converted to LTP in the presence of the TRPV1R antagonist (Fig. 9E,F), a result compatible with the current finding that TRPV1R are inhibitory on BLA-D2 synapses (Fig. 9). We finally controlled for the role of CB1R in BLA-D2 LTD. Bath-application of the SR 141716 ($5 \mu\text{M}$) blocked post-tetanic depression and prevented LTD (Fig. 9E,F), showing that CB1R mediates BLA-D2 LTD.

Discussion

Our principal findings are that in the adult mouse NAc core, the hierarchy of excitatory inputs depends on the identity of the post-synaptic target MSN and on circuit specific properties and that the eCB system endows excitatory circuits of the NAc with pathway-specific plasticity.

Differential intrinsic properties of adult NAc core MSNs

The data show that D1 and D2 MSNs in adult NAc core have distinctive intrinsic properties. Compared with D2, D1 MSNs had a low rheobase, a more depolarized membrane potential and exhibited a higher propensity to trigger action potentials in response to depolarizing current injections. Thus, adult D1 are more excitable than D2 MSNs.

Subtype specific morphological properties (e.g., soma size or dendritic arborization, Gertler et al., 2008) and differences in membrane biophysical properties such as membrane resistance, capacitance, or the expression of voltage-dependent calcium channels, may explain these dissimilarities (Nisenbaum et al., 1994; Hernández-López et al., 1997, 2000).

Divergent intrinsic properties have already been described in juvenile and adolescent mice, however, at these stages D2- are more excitable than D1-MSNs (Kreitzer and Malenka, 2007; Gertler et al., 2008; Ma et al., 2012; Planert et al., 2013; Cao et al., 2018). Although many factors (e.g., recording site, sample size, the presence or absence of TTX, the transgenic mouse line used, the size of the soma or the extent of dendritic arborization) may explain this discrepancy, it is highly probable that age is the determining factor. In keeping with this idea, in rat NAc core, pre-pubertal rats and adult rats display different properties (Belleau and Warren, 2000; Zhang and Warren, 2008; Kasanetz and Manzoni, 2009). Additionally, in both rats and mice, NAc dopamine receptors undergo significant developmental changes during adolescence (Andersen et al., 1997; Andersen and Teicher, 2000).

The subtype specific evolution of excitability in juvenile/adolescent and adults MSNs may be due to differences in membrane resistance and conductance. In support of this possibility, early in development MSNs have very high membrane resistance and do not express inward rectifying potassium channels (Tepper et al., 1998; Belleau and Warren, 2000). The time-scale of this physiological maturation parallels the morphological development of MSNs and dendritic arborization, spine formation and synaptogenesis which continue until the end of the first postnatal month (Tepper et al., 1998; Butler et al., 1999).

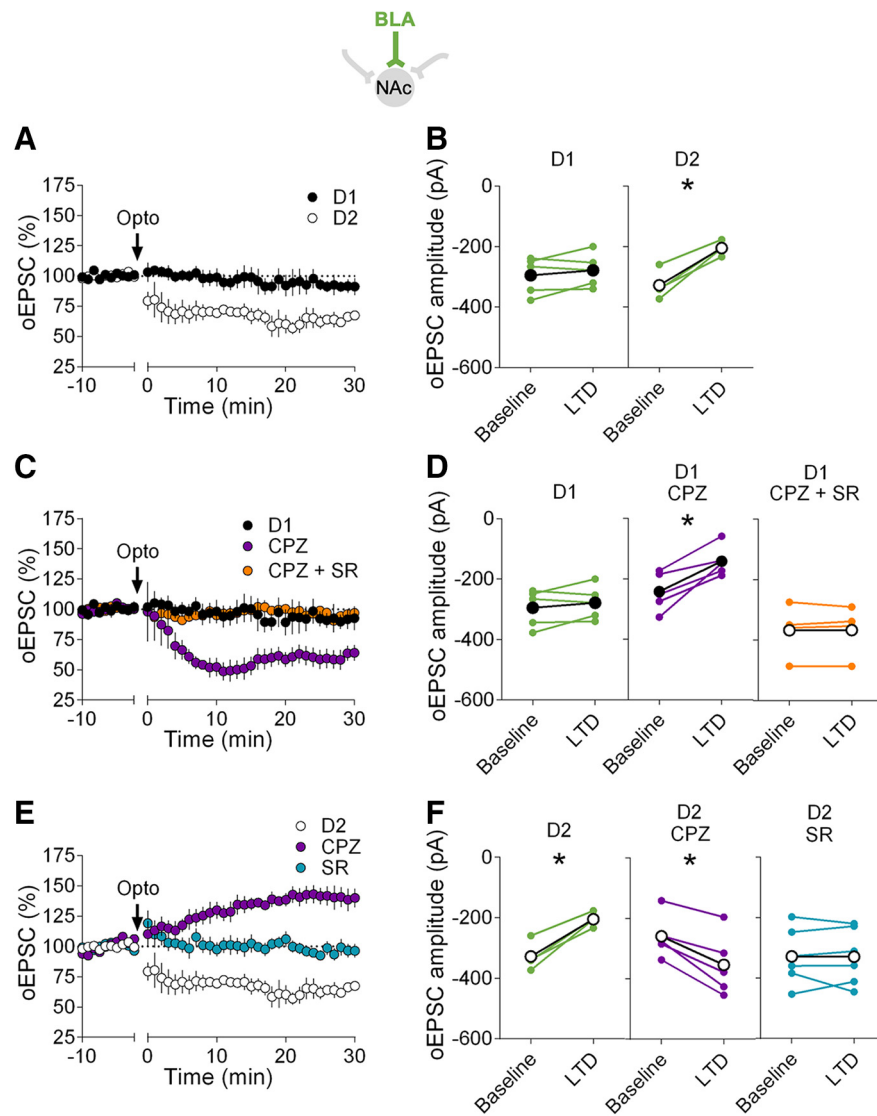


Figure 9. TRPV1R delineates cell-type-specific LTD at amygdala synapses in the NAc core. **A**, Optical stimulation of BLA inputs (10 Hz for 10 min) induced a robust LTD in D2 (white circles, $n = 4$) but not in D1 MSNs (black circles, $n = 5$). **B**, Individual and averaged oEPSC amplitude before (baseline) and 25–30 min after LTD induction (LTD) in D1 and D2 MSNs (D1 MSNs, $p = 0.3311$, D2 MSNs, $p = 0.0072$, paired t test). **C**, Bath perfusion of the TRPV1R capsazepine (CPZ $10 \mu\text{M}$) allowed the induction of LTD at BLA-D1 synapses (purple, $n = 6$; compared with control same as **A**). When CPZ was applied in the presence of the CB1R antagonist SR141716 (SR $5 \mu\text{M}$) LTD induction was prevented (orange, $n = 4$). **D**, Individual and averaged oEPSCs amplitude before (baseline) and 25–30 min after LTD induction (LTD) in D1 MSNs in control, CPZ and CPZ + SR (D1 CPZ, $p = 0.0056$ paired t test; D1 CPZ + SR, $p = 0.9737$). **E**, Antagonism of TRPV1R converted LTD to LTP at BLA-D2 synapses (purple, $n = 5$). Bath application of the CB1R antagonist SR blocked LTD at BLA-D2 synapses (blue, $n = 6$). **F**, Individual and averaged oEPSCs amplitude before (baseline) and 25–30 min after LTD induction (LTD) in D2 MSNs with or without CPZ or SR (D2 CPZ, $p = 0.0068$; SR, $p = 0.9546$ paired t test). n represents the number of mice. All data are shown as mean \pm SEM. * $p < 0.05$ paired t test.

Hierarchy of excitatory afferents depends on MSN subtype in adult NAc core

Pathway-specific opto-stimulation of excitatory inputs in the NAc core revealed that there is a hierarchy of synaptic inputs that depends on the cellular identity of the target MSNs. Most notably, the BLA and the PFC are the main source of synaptic excitation on D1 and D2 neurons, respectively. Similarly, BLA and PFC afferents trigger action potentials with a high probability in D1 and D2 MSNs, respectively.

Differences in the number of fibers per afferent or the amount of glutamate release per fibers may underlie this functional hierarchy. Based on the recent study of Li and colleagues (Li et al.,

2018) that showed similar PFC, BLA, and vHipp innervations of D1 and D2 MSNs, we favor the second proposition.

Input- and synapse-specific function of endocannabinoids

The present data indicate that functional CB1R are present at all synapses tested, albeit with differences in the amount of CB1R-mediated inhibition. The situation was far more complex with TRPV1R. Indeed, a TRPV1R agonist inhibited PFC-evoked oEPSCs in both D1 and D2 MSNs but led to opposite and MSN subtype-specific effects at the BLA pathway: BLA-D1 were enhanced while BLA-D2 synapses were inhibited by capsaicin. TRPV1R specifically inhibited vHipp-D1 synapses and had no effect on vHipp-D2 synapses. Pharmacological activation of TRPV1R suppresses or facilitates neurotransmitter release into the dorsal striatum according to their presynaptic or postsynaptic location (Musella et al., 2009) and our results with sEPSCs also suggest a differential expression of TRPV1R at BLA-D1 and BLA-D2 synapses. Indeed, capsaicin modified the frequency but not the amplitude of sEPSCs in D1 MSNs and vice-versa in D2 MSNs. These data are compatible with presynaptic TRPV1R at BLA-D1 and postsynaptic TRPV1R at BLA-D2 synapses. Grueter et al. (2010) also reported a postsynaptic localization of TRPV1R at D2 MSNs.

At the BLA-NAc pathway, TRPV1R and CB1R modulate synaptic transmission in a cell specific manner: LTD could be induced in D2 but not in D1 MSNs in agreement with a previous report where the identity of MSNs was not ascertained (Grueter et al., 2010). At first glance, these results may be taken as an indication that BLA-D2 MSNs are incapable of expressing eCB-LTD. However, the current pharmacological characterization and previous work (Neuhofer et al., 2018) led us to hypothesize that the tetanus-induced eCB (presumably anandamide) activates TRPV1R and that the ensuing potentiation masked/prevented LTD.

In support of this idea, we observed that, in the presence of a TRPV1R antagonist, the previously inefficient protocol triggered a large LTD. The mirror situation was observed at BLA-D2 synapses where LTD was converted to LTP in the presence of the TRPV1R antagonist.

In summary, our study reveals the cell-type-specific synaptic organization of hippocampal, amygdala and prefrontal inputs to the PFC. It is tempting to speculate that pathway and cell specific synaptic strengths correlate with distinct functions and associated behaviors. Future work will determine whether the PFC-D2 “dominant pathway” is preferentially engaged in executive functions and the role of the BLA-D1 pathway in emotional behav-

iors. In this context, the observation that two subpopulations of BLA glutamatergic neurons project to NAc core D1 or D2 MSNs to generate emotional responses of opposite valence is an indication of similar parallel dual control circuits at PFC- and/or vHipp-NAc pathways (Shen et al., 2019).

Moreover, these data highlight the versatility of the endocannabinoid system in shaping activity-dependent synaptic plasticity at BLA-NAc circuits and cortical-limbic circuits in general.

In conclusion, our experiments reveal a high degree of synapse and circuit specificity in the adult NAc core and illustrate how endocannabinoids contribute to pathway-specific synaptic plasticity.

References

- Abela AR, Duan Y, Chudasama Y (2015) Hippocampal interplay with the nucleus accumbens is critical for decisions about time. *Eur J Neurosci* 42:2224–2233.
- Ade KK, Wan Y, Chen M, Gloss B, Calakos N (2011) An improved bac transgenic fluorescent reporter line for sensitive and specific identification of striatonigral medium spiny neurons. *Front Syst Neurosci* 5:32.
- Ambroggi F, Ishikawa A, Fields HL, Nicola SM (2008) Basolateral amygdala neurons facilitate reward-seeking behavior by exciting nucleus accumbens neurons. *Neuron* 59:648–661.
- Andersen SL, Teicher MH (2000) Sex differences in dopamine receptors and their relevance to ADHD. *Neurosci Biobehav Rev* 24:137–141.
- Andersen SL, Rutstein M, Benzo JM, Hostetter JC, Teicher MH (1997) Sex differences in dopamine receptor overproduction and elimination. *Neuroreport* 8:1495–1498.
- Araque A, Castillo PE, Manzoni OJ, Tonini R (2017) Synaptic functions of endocannabinoid signaling in health and disease. *Neuropharmacology* 124:13–24.
- Bara A, Manduca A, Bernabeu A, Borsoi M, Serviado M, Lassalle O, Murphy M, Wager-Miller J, Mackie K, Pelissier-Alicot AL, Trezza V, Manzoni OJ (2018) Sex-dependent effects of in utero cannabinoid exposure on cortical function. *Elife* 7:e36234.
- Belleau ML, Warren RA (2000) Postnatal development of electrophysiological properties of nucleus accumbens neurons. *J Neurophysiol* 84:2204–2216.
- Bertran-Gonzalez J, Bosch C, Maroteaux M, Matamalas M, Hervé D, Valjent E, Girault JA (2008) Opposing patterns of signaling activation in dopamine D1 and D2 receptor-expressing striatal neurons in response to cocaine and haloperidol. *J Neurosci* 28:5671–5685.
- Beyeler A, Namburi P, Globler GF, Simonnet C, Calhoun GG, Conyers GF, Luck R, Wildes CP, Tye KM (2016) Divergent routing of positive and negative information from the amygdala during memory retrieval. *Neuron* 90:348–361.
- Beyeler A, Chang CJ, Silvestre M, Lévêque C, Namburi P, Wildes CP, Tye KM (2018) Organization of valence-encoding and projection-defined neurons in the basolateral amygdala. *Cell Rep* 22:905–918.
- Bosch-Bouju C, Larriou T, Linders L, Manzoni OJ, Layé S (2016) Endocannabinoid-mediated plasticity in nucleus accumbens controls vulnerability to anxiety after social defeat stress. *Cell Rep* 16:1237–1242.
- Britt JP, Benaliouad F, McDevitt RA, Stuber GD, Wise RA, Bonci A (2012) Synaptic and behavioral profile of multiple glutamatergic inputs to the nucleus accumbens. *Neuron* 76:790–803.
- Butler AK, Uryu K, Rougon G, Chesselet MF (1999) N-methyl-D-aspartate receptor blockade affects polysialylated neural cell adhesion molecule expression and synaptic density during striatal development. *Neuroscience* 89:1169–1181.
- Cao J, Dorris DM, Meitzen J (2018) Electrophysiological properties of medium spiny neurons in the nucleus accumbens core of prepubertal male and female *Drd1a*-tdTomato line 6 BAC transgenic mice. *J Neurophysiol* 120:1712–1727.
- Cardinal RN, Howes NJ (2005) Effects of lesions of the nucleus accumbens core on choice between small certain rewards and large uncertain rewards in rats. *BMC Neuroscience* 6:37.
- Christakou A, Robbins TW, Everitt BJ (2001) Functional disconnection of a prefrontal cortical–dorsal striatal system disrupts choice reaction time performance: implications for attentional function. *Behav Neurosci* 115:812–825.
- Christakou A, Robbins TW, Everitt BJ (2004) Prefrontal cortical–ventral striatal interactions involved in affective modulation of attentional performance: implications for corticostriatal circuit function. *J Neurosci* 24:773–780.
- Cools R, Sheridan M, Jacobs E, D’Esposito M (2007) Impulsive personality predicts dopamine-dependent changes in frontostriatal activity during component processes of working memory. *J Neurosci* 27:5506–5514.
- Eichenbaum H (2014) Time cells in the hippocampus: a new dimension for mapping memories. *Nat Rev Neurosci* 15:732–744.
- Enoksson T, Bertran-Gonzalez J, Christie MJ (2012) Nucleus accumbens D2- and D1-receptor expressing medium spiny neurons are selectively activated by morphine withdrawal and acute morphine, respectively. *Neuropharmacology* 62:2463–2471.
- Everitt BJ, Morris KA, O’Brien A, Robbins TW (1991) The basolateral amygdala-ventral striatal system and conditioned place preference: further evidence of limbic-striatal interactions underlying reward-related processes. *Neuroscience* 42:1–18.
- Everitt BJ, Cardinal RN, Parkinson JA, Robbins TW (2003) Appetitive behavior. *Ann N Y Acad Sci* 985:233–250.
- Fernando AB, Murray JE, Milton AL (2013) The amygdala: securing pleasure and avoiding pain. *Front Behav Neurosci* 7:190.
- Finch DM (1996) Neurophysiology of converging synaptic inputs from the rat prefrontal cortex, amygdala, midline thalamus, and hippocampal formation onto single neurons of the caudate/putamen and nucleus accumbens. *Hippocampus* 6:495–512.
- Floresco SB (2015) The nucleus accumbens: an interface between cognition, emotion, and action. *Annu Rev Psychol* 66:25–52.
- Floresco SB, Seamans JK, Phillips AG (1997) Selective roles for hippocampal, Prefrontal Cortical, and Ventral Striatal Circuits in Radial-Arm Maze Tasks With or Without a Delay. *J Neurosci* 17:1880–1890.
- Floresco SB, Braakma DN, Phillips AG (1999) Thalamic–cortical–striatal circuitry subserves working memory during delayed responding on a radial arm maze. *J Neurosci* 19:11061–11071.
- Francis TC, Chandra R, Friend DM, Finkel E, Dayrit G, Miranda J, Brooks JM, Iniguez SD, O’Donnell P, Kravitz A, Lobo MK (2015) Nucleus accumbens medium spiny neuron subtypes mediate depression-related outcomes to social defeat stress. *Biol Psychiatry* 77:212–222.
- French SJ, Totterdell S (2002) Hippocampal and prefrontal cortical inputs monosynaptically converge with individual projection neurons of the nucleus accumbens. *J Comp Neurol* 446:151–165.
- French SJ, Totterdell S (2003) Individual nucleus accumbens-projection neurons receive both basolateral amygdala and ventral subicular afferents in rats. *Neuroscience* 119:19–31.
- Gerdeman GL, Ronesi J, Lovinger DM (2002) Postsynaptic endocannabinoid release is critical to long-term depression in the striatum. *Nat Neurosci* 5:446–451.
- Gertler TS, Chan CS, Surmeier DJ (2008) Dichotomous anatomical properties of adult striatal medium spiny neurons. *J Neurosci* 28:10814–10824.
- Gibson HE, Edwards JG, Page RS, Van Hook MJ, Kauer JA (2008) TRPV1 channels mediate long-term depression at synapses on hippocampal interneurons. *Neuron* 57:746–759.
- Goda Y, Stevens CF (1994) Two components of transmitter release at a central synapse. *Proc Natl Acad Sci U S A* 91:12942–12946.
- Goto Y, Grace AA (2008) Limbic and cortical information processing in the nucleus accumbens. *Trends Neurosci* 31:552–558.
- Groenewegen HJ, Wright CI, Beijer AV, Voorn P (1999) Convergence and segregation of ventral striatal inputs and outputs. *Ann N Y Acad Sci* 877:49–63.
- Grueter BA, Brasnjo G, Malenka RC (2010) Postsynaptic TRPV1 triggers cell type-specific long-term depression in the nucleus accumbens. *Nat Neurosci* 13:1519–1525.
- Hernández-López S, Bargas J, Surmeier DJ, Reyes A, Galarraga E (1997) D1 receptor activation enhances evoked discharge in neostriatal medium spiny neurons by modulating an L-type Ca²⁺ conductance. *J Neurosci* 17:3334–3342.
- Hernández-López S, Tkatch T, Perez-Garci E, Galarraga E, Bargas J, Hamm H, Surmeier DJ (2000) D2 dopamine receptors in striatal medium spiny neurons reduce L-type Ca²⁺ currents and excitability via a novel PLCβ1–IP3–calcineurin-signaling cascade. *J Neurosci* 20:8987–8995.
- Humphries MD, Prescott TJ (2010) The ventral basal ganglia, a selection mechanism at the crossroads of space, strategy, and reward. *Prog Neurobiol* 90:385–417.
- Ito R, Robbins TW, Pennartz CM, Everitt BJ (2008) Functional interaction between the hippocampus and nucleus accumbens shell is necessary for

- the acquisition of appetitive spatial context conditioning. *J Neurosci* 28:6950–6959.
- Jung KM, Sepers M, Henstridge CM, Lassalle O, Neuhof D, Martin H, Ginger M, Frick A, DiPatrizio NV, Mackie K, Katona I, Piomelli D, Manzoni OJ (2012) Uncoupling of the endocannabinoid signalling complex in a mouse model of fragile X syndrome. *Nat Commun* 3:1080.
- Kasanetz F, Manzoni OJ (2009) Maturation of excitatory synaptic transmission of the rat nucleus accumbens from juvenile to adult. *J Neurophysiol* 101:2516–2527.
- Kasanetz F, Deroche-Gamonet V, Berson N, Balado E, Lafourcade M, Manzoni O, Piazza PV (2010) Transition to addiction is associated with a persistent impairment in synaptic plasticity. *Science* 328:1709–1712.
- Kreitzer AC, Malenka RC (2007) Endocannabinoid-mediated rescue of striatal LTD and motor deficits in Parkinson's disease models. *Nature* 445:643–647.
- Lafourcade M, Elezgarai I, Mato S, Bakiri Y, Grandes P, Manzoni OJ (2007) Molecular components and functions of the endocannabinoid system in mouse prefrontal cortex. *PLoS One* 2:e709.
- Lafourcade M, Larrieu T, Mato S, Duffaud A, Sepers M, Matias I, De Smedt-Peyrusse V, Labrousse VF, Bretillon L, Matute C, Rodríguez-Puertas R, Layé S, Manzoni OJ (2011) Nutritional omega-3 deficiency abolishes endocannabinoid-mediated neuronal functions. *Nat Neurosci* 14:345–350.
- LeDoux J (2003) The emotional brain, fear, and the amygdala. *Cell Mol Neurobiol* 23:727–738.
- Li Z, Chen Z, Fan G, Li A, Yuan J, Xu T (2018) Cell-type-specific afferent innervation of the nucleus accumbens core and shell. *Front Neuroanat* 12:84.
- Lobo MK, Nestler EJ (2011) The striatal balancing act in drug addiction: distinct roles of direct and indirect pathway medium spiny neurons. *Front Neuroanat* 5:41.
- Ma YY, Cepeda C, Chatta P, Franklin L, Evans CJ, Levine MS (2012) Regional and cell-type-specific effects of DAMGO on striatal D1 and D2 dopamine receptor-expressing medium-sized spiny neurons. *ASN Neuro* 4:e00077.
- Ma YY, Lee BR, Wang X, Guo C, Liu L, Cui R, Lan Y, Balcita-Pedico JJ, Wolf ME, Sesack SR, Shaham Y, Schlüter OM, Huang YH, Dong Y (2014) Bidirectional modulation of incubation of cocaine craving by silent synapse-based remodeling of prefrontal cortex to accumbens projections. *Neuron* 83:1453–1467.
- Manduca A, Bara A, Larrieu T, Lassalle O, Joffre C, Layé S, Manzoni OJ (2017) Amplification of mGlu5-endocannabinoid signaling rescues behavioral and synaptic deficits in a mouse model of adolescent and adult dietary polyunsaturated fatty acid imbalance. *J Neurosci* 37:6851–6868.
- Mannella F, Gurney K, Baldassarre G (2013) The nucleus accumbens as a nexus between values and goals in goal-directed behavior: a review and a new hypothesis. *Front Behav Neurosci* 7:135.
- Martin HGS, Lassalle O, Manzoni OJ (2017) Differential adulthood onset mGlu5 signaling saves prefrontal function in the fragile X mouse. *Cereb Cortex* 27:5592–5602.
- McGarry LM, Carter AG (2017) Prefrontal cortex drives distinct projection neurons in the basolateral amygdala. *Cell Rep* 21:1426–1433.
- McGinty VB, Grace AA (2009) Timing-dependent regulation of evoked spiking in nucleus accumbens neurons by integration of limbic and prefrontal cortical inputs. *J Neurophysiol* 101:1823–1835.
- McLaughlin RJ, Floresco SB (2007) The role of different subregions of the basolateral amygdala in cue-induced reinstatement and extinction of food-seeking behavior. *Neuroscience* 146:1484–1494.
- Micale V, Cristino L, Tamburella A, Petrosino S, Leggio GM, Drago F, Di Marzo V (2009) Anxiolytic effects in mice of a dual blocker of fatty acid amide hydrolase and transient receptor potential vanilloid type-1 channels. *Neuropsychopharmacology* 34:593–606.
- Musella A, De Chiara V, Rossi S, Prosperetti C, Bernardi G, Maccarrone M, Centonze D (2009) TRPV1 channels facilitate glutamate transmission in the striatum. *Mol Cell Neurosci* 40:89–97.
- Neuhof D, Henstridge CM, Dudok B, Sepers M, Lassalle O, Katona I, Manzoni OJ (2015) Functional and structural deficits at accumbens synapses in a mouse model of Fragile X. *Front Cell Neurosci* 9:100.
- Neuhof D, Lassalle O, Manzoni OJ (2018) Muscarinic M1 receptor modulation of synaptic plasticity in nucleus accumbens of wild-type and fragile X mice. *ACS Chem Neurosci* 9:2233–2240.
- Nisenbaum ES, Xu ZC, Wilson CJ (1994) Contribution of a slowly inactivating potassium current to the transition to firing of neostriatal spiny projection neurons. *J Neurophysiol* 71:1174–1189.
- Planert H, Berger TK, Silberberg G (2013) Membrane properties of striatal direct and indirect pathway neurons in mouse and rat slices and their modulation by dopamine. *PLoS One* 8:e57054.
- Qi J, Zhang S, Wang HL, Barker DJ, Miranda-Barrientos J, Morales M (2016) VTA glutamatergic inputs to nucleus accumbens drive aversion by acting on GABAergic interneurons. *Nat Neurosci* 19:725–733.
- Robbe D, Alonso G, Duchamp F, Bockaert J, Manzoni OJ (2001) Localization and mechanisms of action of cannabinoid receptors at the glutamatergic synapses of the mouse nucleus accumbens. *J Neurosci* 21:109–116.
- Robbe D, Kopf M, Remaury A, Bockaert J, Manzoni OJ (2002) Endogenous cannabinoids mediate long-term synaptic depression in the nucleus accumbens. *Proc Natl Acad Sci U S A* 99:8384–8388.
- Rogers-Carter MM, Djerdjaj A, Gribbons KB, Varela J, Christianson JP (2019) Insular cortex projections to nucleus accumbens core mediate social approach to stressed juvenile rats. Available at <http://biorxiv.org/lookup/doi/10.1101/544221>.
- Salgado S, Kaplitt MG (2015) The nucleus accumbens: a comprehensive review. *Stereotactic and Functional Neurosurgery* 93:75–93.
- Sesack SR, Grace AA (2010) Cortico-basal ganglia reward network: microcircuitry. *Neuropsychopharmacology* 35:27–47.
- Shen CJ, Zheng D, Li KX, Yang JM, Pan HQ, Yu XD, Fu JY, Zhu Y, Sun QX, Tang MY, Zhang Y, Sun P, Xie Y, Duan S, Hu H, Li XM (2019) Cannabinoid CB1 receptors in the amygdalar cholecystokinin glutamatergic afferents to nucleus accumbens modulate depressive-like behavior. *Nat Med* 25:337–349.
- Shiflett MW, Balleine BW (2010) At the limbic-motor interface: disconnection of basolateral amygdala from nucleus accumbens core and shell reveals dissociable components of incentive motivation. *Eur J Neurosci* 32:1735–1743.
- Silver RA, Momiyama A, Cull-Candy SG (1998) Locus of frequency-dependent depression identified with multiple-probability fluctuation analysis at rat climbing fibre-Purkinje cell synapses. *J Physiol* 510:881–902.
- Stratford TR, Wirtshafter D (2013) Injections of muscimol into the paraventricular thalamic nucleus, but not mediadorsal thalamic nuclei, induce feeding in rats. *Brain Res* 1490:128–133.
- Tepper JM, Sharpe NA, Koós TZ, Trent F (1998) Postnatal development of the rat neostriatum: electrophysiological, light- and electron-microscopic studies. *Dev Neurosci* 20:125–145.
- Thibault D, Loustalot F, Fortin GM, Bourque MJ, Trudeau LÉ (2013) Evaluation of D1 and D2 dopamine receptor segregation in the developing striatum using BAC transgenic mice. *PLoS One* 8:e67219.
- Thomazeau A, Lassalle O, Iafrati J, Souchet B, Guedj F, Janel N, Chavis P, Delabar J, Manzoni OJ (2014) Prefrontal deficits in a murine model overexpressing the down syndrome candidate gene *dyr1a*. *J Neurosci* 34:1138–1147.
- Thomazeau A, Bosch-Bouju C, Manzoni O, Layé S (2017) Nutritional n-3 PUFA deficiency abolishes endocannabinoid gating of hippocampal long-term potentiation. *Cereb Cortex* 27:2571–2579.
- Trouche S, Koren V, Doig NM, Ellender TJ, El-Gaby M, Lopes-Dos-Santos V, Reeve HM, Perestenko PV, Garas FN, Magill PJ, Sharott A, Dupret D (2019) A Hippocampus-Accumbens Tripartite Neuronal Motif Guides Appetitive Memory in Space. *Cell* 176:1393–1406.
- Tye KM, Prakash R, Kim SY, Fenno LE, Grosenick L, Zarabi H, Thompson KR, Gradinaru V, Ramakrishnan C, Deisseroth K (2011) Amygdala circuitry mediating reversible and bidirectional control of anxiety. *Nature* 471:358–362.
- Wu YW, Kim JI, Tawfik VL, Lalchandani RR, Scherrer G, Ding JB (2015) Input- and cell-type-specific endocannabinoid-dependent LTD in the striatum. *Cell Rep* 10:75–87.
- Yizhar O, Fenno LE, Davidson TJ, Mogri M, Deisseroth K (2011) Optogenetics in neural systems. *Neuron* 71:9–34.
- Zahm DS, Brog JS (1992) On the significance of subterritories in the “accumbens” part of the rat ventral striatum. *Neuroscience* 50:751–767.
- Zhang L, Warren RA (2008) Postnatal development of excitatory postsynaptic currents in nucleus accumbens medium spiny neurons. *Neuroscience* 154:1440–1449.
- Zhu Y, Wienecke CF, Nachtrab G, Chen X (2016) A thalamic input to the nucleus accumbens mediates opiate dependence. *Nature* 530:219–222.